Kinetics of Channeling Cracks in Polymeric Coatings

Fanbo Meng[a], J. L. David[b], S. Bollin[c], M. E. Nichols[c]
and M. D. Thouless[a,d,1]

[a]*Department of Mechanical Engineering, University of Michigan, Ann Arbor, MI 48109, USA*
[b]*Momentive Performance Materials Inc., Waterford, NY 12188, USA*
[c]*Research and Advanced Engineering, Ford Motor Company, Dearborn, MI 48124, USA*
[d]*Department of Materials Science and Engineering, University of Michigan, Ann Arbor, MI 48109, USA*

Abstract

Techniques to measure the relationship between crack velocity and energy-release rate for channeling cracks in thin films and coatings are presented in this paper. The approach uses linear-elastic fracture mechanics to relate the crack spacing, material properties and geometry to the energy-release rate of a channeling crack, by means of detailed finite-element calculations. The velocities of individual cracks are monitored and related to their distance to nearest neighbors as part of these calculations. Other parameters that were identified as being important in determining the energy-release rate were the depth below the surface to which the crack penetrated, and the residual strain in the cracked layer. A technique to determine the crack depth was developed which involved focused-ion beam milling of the specimen, followed by electron microscopy. The residual strain in the crack layer was determined by measuring the crack-mouth opening using atomic-force microscopy, and comparing this to numerical analyses.

These approaches were used to analyze a multi-layer system consisting of a polymeric, colloidal-silica nano-composite layer and a primer layer coating a polycarbonate substrate. The crack growth showed a threshold value of energy-release rate corresponding to about 6.6 J/m^2, with a minimum detectable crack velocity of about 3 nm/s. When the energy-release rate was increased to about 25 J/m^2, the resultant crack velocity was 10^{-2} m/s. The channeling cracks in this system exhibited the characteristics of a thermally-activated rupture process, but showed no evidence of fatigue or stress-corrosion cracking under the conditions studied.

August 23, 2017

Keywords: polymer coatings, crack velocity, channeling, kinetics, threshold

[1]Corresponding author: (001)734-763-5289 (thouless@umich.edu)

1 Introduction

The replacement of glass by transparent polymers, such as polycarbonates, has many advantages for automotive applications. Lower densities permit lighter-weight, energy-efficient structures. Alternative processing routes allow for more creative designs. There are, however, two major limitations with the use of polymers for automotive glazing. The first is their vulnerability to ultra-violet light, which can cause embrittlement and discoloration. The second is their relative softness, which results in them being very easy to scratch. Both of these limitations can be overcome by the application of nano-composite coatings containing a hard wear-resistant phase and ultra-violet absorbers. However, the intrinsic hardness of these coatings makes them vulnerable to failure by fracture over prolonged service conditions [1]. Therefore, the motivation for this paper was to explore the phenomenon of time-dependent fracture in nano-composite coatings on polymer substrates.

Cracking induced by uniaxial tensile stresses in a coating on a substrate occurs by a mechanism known as channeling; this results in a series of parallel cracks propagating across the coating. The basic fracture mechanics for this problem in an elastic system is well understood. For example, the energy-release rate for a single crack channeling across a coating of thickness h_c on a very tough substrate of thickness H, and subjected to a uniform tensile strain of ε_o, is of the form [2, 3]

$$\mathcal{G} = \varepsilon_o^2 \bar{E}_c h_c \; f_D\left(\tilde{\alpha}, \tilde{\beta}, h_c/H\right). \tag{1}$$

In this equation, $\bar{E}_c = E_c/(1-\nu_c^2)$, is the plane-strain Young's modulus of the coating, ν_c is Poisson's ratio, and $f_D\left(\tilde{\alpha}, \tilde{\beta}, h_c/H\right)$ is a function of the two Dundurs' parameters, $\tilde{\alpha}$ and $\tilde{\beta}$, which are measures of the elastic mismatch between the coating and substrate, and

the ratio of coating and substrate thicknesses. The Dundurs' parameters are given by [4]

$$\tilde{\alpha} = \frac{\bar{E}_c - \bar{E}_s}{\bar{E}_c + \bar{E}_s} \tag{2}$$

and

$$\tilde{\beta} = \frac{\bar{E}_c(1-\bar{\nu}_s) - \bar{E}_s(1-\bar{\nu}_c)}{2(\bar{E}_c + \bar{E}_s)} \tag{3}$$

where, $\bar{\nu}_c = \nu_c/(1-\nu_c)$ is the plane-strain Poisson's ratio for the coating, and $\bar{E}_s$ and $\bar{\nu}_s$ are the plane-strain modulus and the plane-strain Poisson's ratio, respectively, for the substrate. A single crack propagates if the energy-release rate exceeds the toughness of the coating, Γ_c. Additional cracks can grow at higher levels of the energy-release rate, forming patterns of parallel cracks. The density of the cracks increases with applied strain [5, 6, 7]; it also depends on the modulus ratio [8] and toughness [9] mismatch between the coating and substrate, and on the statistics of the initial flaw population [10].

A coating will remain crack-free during service, provided the value of the energy-release rate (Eqn. 1) is always less than the toughness of the coating. However, cracks can develop during service for a variety of reasons. A build up of stress could increase the energy-release rate. Degradation of the coating could decrease the toughness. Cyclic loading could result in sub-critical fatigue-crack initiation and growth. Stress-corrosion, creep, or visco-elastic effects could induce time-dependent crack growth. It is the time-dependent and fatigue aspects of the problem that were explored in this study.

Time-dependent crack growth can occur if the constraint on a coating is gradually relaxed by creep of the substrate, or of the primer layer [11, 12]. This is because both creep and visco-elastic relaxation lower the effective modulus of a material, and the energy-release rate for channeling in a coating increases with the compliance of the material beneath it [2]. For example, if one were to model the substrate as a standard-linear solid, one

could consider two limiting values for its modulus [13]: a higher, unrelaxed modulus at short time scales, and a lower, relaxed modulus at long time scales. If the energy-release rate for channeling associated with the unrelaxed substrate modulus exceeds the coating toughness, Γ_c, spontaneous fracture occurs. If the energy-release rate for channeling associated with the relaxed substrate modulus is less than Γ_c, fracture will never occur. In between this range of energy-release rates, the crack will channel across the coating at a steady-state velocity associated with a time scale corresponding to the effective modulus that makes $\mathcal{G} = \Gamma_c$.

Time-dependent crack growth associated with visco-elastic effects in the coating itself would not seem to be possible, although it does occur in visco-elastic materials under load control. Under these conditions, a lower threshold for crack growth is associated with the fully-relaxed modulus of the coating, and an upper threshold for crack growth is associated with the unrelaxed modulus [14]. However, under the strain-controlled conditions of a visco-elastic coating bonded to an elastic substrate, the drop in modulus with time would not result in such behavior, as it would cause the energy-release rate to decrease with a drop in crack velocity.

Stress-corrosion cracking can cause time-dependent crack growth [15]. This has been shown to occur in silica-containing coatings [16] and in silicon-nitride films [17, 18]. It has also been shown to be an issue for delamination of silica-containing films [19, 20, 21]. Like visco-elastic crack growth, stress-corrosion cracking occurs within a limited range of energy-release rate. There is an upper threshold when the crack grows so quickly that there is no time for the crack tip to interact with the environment (such as water vapor). There is a lower threshold when the crack grows so slowly that the crack tip is essentially in equilibrium with the environment. corresponding to slow crack growth in which the environment

(such as water vapor) can interact with the bonds at the crack tip, essentially lowering the toughness of the coating. Between these limits the crack velocity depends either on how quickly the environment can reach the crack tip, or on the rate of reaction between the environment and the atoms or molecules at the crack tip [22, 23]. There is also a higher threshold, corresponding to crack growth in a vacuum. Stress-corrosion cracking can be identified by any observed effect of the environment on crack velocity, and by the existence of these upper and lower thresholds.

Crack growth in solids is always associated with the rupture of bonds or the pullout of molecules. These are thermally-activated processes, so crack growth is inherently a time-dependent phenomenon, even in the absence of environmental effects[2]. For example, while stress-corrosion cracking is a thermally-activated process, so is crack growth in a vacuum [24]. However, the activation energies and other parameters may not always be in a range for the time-dependent nature of crack growth to be manifested. A thermodynamic model of fracture has been developed by Lawn [25]; this relates the crack velocity, v, to the energy-release rate, $\mathcal{G}$, and the toughness of the coating, Γ_c. In this model, the driving force for thermally-activated rupture at the crack tip is the difference between the energy-release rate and the intrinsic toughness of the material. At equilibrium, the energy-release rate equals the toughness, and the rate of bond rupture equals the rate of bond healing, so no crack propagation occurs. This corresponds to a threshold energy-release rate for fracture. Above this threshold, the driving force for rupture increases, and the crack velocity increases exponentially with energy-release rate. Thermal-activation of rupture also results in an exponential increase in velocity with temperature. The crack velocity is

[2] Although not discussed specifically, there seems to be evidence of thermally-activated crack growth in the absence of environmental effects in the studies of Refs. [17] and [18].

given by

$$v = A \exp\left(-Q/kT\right) \sinh\left[B\left(\mathcal{G} - \Gamma_c\right)/kT\right], \tag{4}$$

where k is Boltzmann's constant, T is the absolute temperature, Q is the activation energy for the rupture process. The parameters A and B are related to the discrete increments of length over which rupture can occur, such as atomic spacing, both in the direction of crack advance and perpendicular to it. The parameter A is given by $A \approx kT\Delta_x/\pi\hbar$, where Δ_x is the characteristic length in the direction of crack growth and $\hbar$ is the Dirac constant. The parameter B is given by $B \approx \Delta_x\Delta_y/2$, where Δ_y is the characteristic length parallel to the crack tip. In the absence of environmental effects, this kinetic model exhibits only a lower threshold associated with equilibrium.

In this paper, we explore channel cracking in a nano-composite coating on polycarbonate. Empirical observations had shown that exposure to service conditions resulted in the formation of such cracks after a period of time. This provided the original motivation behind the study: to try and elucidate what might be the nature of any time-dependent crack growth. Therefore, we developed a technique, based on fracture mechanics, to measure crack velocities as a function of energy-release rate in coatings. We showed that the crack velocity had the form expected from Lawn's kinetic model, for which we could obtain material parameters associated with the fracture process. From a practical perspective, we also demonstrated that there was no fatigue or stress-corrosion cracking in the particular system described in this paper.

2 Experiments

2.1 Material properties

Clear polycarbonate sheets with a thickness of 3.0 ± 0.02 mm were coated with a thermally-cured, silicone topcoat (or hardcoat) on a polyacrylate-based primer (Fig. 1). The topcoat was filled with colloidal silica, and had a thickness of 6.1 ± 0.6 μm thick; the primer had a thickness of 1.4 ± 0.4 μm.

Single layers of the topcoat and primer were coated on polished, 16-gauge, brass discs to measure the temperature-dependent mechanical properties of the layers. Brass was used to ensure good thermal transfer between the heating stage and the material being tested. The fabrication procedures for these specimens were identical to those used for preparing coatings on the polycarbonate substrates, but the thickness of each coating was approximately 6 μm, to facilitate the measurements. Dynamic indentation tests were performed using a Hysitron TI 950 TriboIndenter™ with a diamond Berkovich probe, at testing depths of approximately 5% of the layer thicknesses. The measurements were conducted at frequencies of 10 Hz and 200 Hz, over a temperature range of 25 °C to 120 °C. The resultant values for the storage modulus and loss tangent of both layers are given in Fig. 2.

The temperature-dependent properties of the substrate were measured by dynamic-mechanical analysis (DMA), using a TA Instruments® RSA3 solid analyzer. A sinusoidal compressive load at a frequency of 1 Hz was applied to an uncoated substrate, inducing compressive strains between 0.8% and 0.1%. The loss modulus, the storage modulus, and the loss tangent corresponding to this frequency are presented in Fig. 3 for a range of temperatures up to 150 °C.

2.2 Crack velocity

The coated sheets of polycarbonate were cut into 22 mm $\times$ 155 mm rectangular sections, and the cut edges were milled. An MTS 858 Bionix II tensile machine was used to apply a uniaxial tensile strain in the range of 0.75% to 1.65%. The strain was applied at different nominal strain rates over the range of 0.5×10^{-4} s^{-1} to 2×10^{-4} s^{-1}, and then held at different levels while crack growth occurred. The experiments were conducted at temperatures of 25 ± 2 °C, 48 ± 2 °C, 65 ± 3 °C and 89 ± 3 °C, at ambient relative humidity (which varied from 16% to 33%). An additional set of experiments was conducted to investigate the effects of humidity at room temperature, using three different humidities of $19 \pm 3\%$, $29 \pm 4\%$ and $61 \pm 4\%$. No obvious effects of humidity were observed from these experiments.

A series of optical micrographs were taken during the course of the experiments, both during the loading process, and while the strain was held constant. The strains in the coatings were determined by digital-image-correlation (DIC), with the relative displacement of markers on the surfaces of the coatings being analyzed using a commercial software package (MetaMorph®). The crack spacings were measured from the optical images. The crack velocities were determined by measuring the changes in position of crack tips as a function of time. The crack velocities for a given crack were fairly constant, although some minor variations were observed that probably corresponded to local changes in the thickness of the topcoat.

Examples of the type of images used for the optical measurements are given in Fig. 4. In this figure, two cracks can be seen propagating in opposite directions between two established cracks. The energy-release rate, and hence the crack speed, depends on the distance

of a propagating crack from its nearest neighbors. For a given level of applied strain, the energy-release rate is higher when the spacing is larger, as discussed in the Section 3. In the example shown in Fig. 4, the cracks slowed down after the tips of the propagating cracks passed one another, because their own interactions formed a new nearest-neighbor spacing.

Cyclic loading may cause cracks to propagate by fatigue. However, to verify fatigue, the effects of kinetic growth need to be deconvoluted from any possible fatigue growth. To do this, one needs to determine whether the crack velocity under cyclic conditions is faster than would be expected by merely integrating the kinetic contribution to crack growth, and whether there is any effect of frequency on the velocity. Possible effects of fatigue were investigated by measuring the crack velocities while cycling the specimen under zero-to-tension conditions at 1 Hz, 2 Hz and 5 Hz with mean strains of $0.97 \pm 0.03\%$ at 24 ± 1 °C. The crack velocities observed in these experiments were compared to the crack velocities measured in the static experiments at a corresponding level of average strain. No effect of fatigue greater than the level of the experimental uncertainties was found for these samples.

2.3 Crack depth

The energy-release rate for channeling depends on the crack depth. Therefore, it is important to know whether the cracks penetrate beyond the topcoat, into the primer or substrate. The crack depth was found by using a focused Ga-ion beam (5.0 kV voltage and 0.4 nA) to make cross-sections through cracked portions of the coating, and examining the section by scanning-electron microscopy (SEM). An example of a resulting image is shown in Fig. 5 for a specimen with a 6.3 μm thick topcoat and a 1.4 μm thick primer. This image clearly shows that the channeling crack terminated at the interface between the topcoat and primer. This observation was consistent between several such sections. It should also be noted that

the observation that the crack does not extend into the primer is consistent with the predictions of linear-elastic fracture mechanics [2], in that the modulus of the topcoat is slightly lower than that of the primer.

2.4 Residual tension

Accurate calculations for the energy-release rate of channeling cracks requires a knowledge of the residual strain in the coating caused by the initial curing and processing. This was estimated at room temperature by using atomic-force microscopy (AFM) to measure residual crack openings at the surface of the coating, after the applied strain had been removed. Samples were examined with a Bruker© Multimode AFM equipped with a Nanoscope® V controller in tapping mode, using TESP tips. An example of the experimental results is shown in Fig. 6. The AFM trace corresponds to a line across the middle crack in a set of three (identified as crack "2" in Fig. 6(a)). It should be noted that the crack opening at the surface can be measured quite accurately by AFM, but the full crack profile shown in Fig. 6(b) is not accurate because of the finite size of the AFM tip. The crack is relatively narrow, and the AFM tip cannot penetrate very far into the crack. However, this does not matter because it is only the crack-mouth opening that is used to deduce the residual tension.

In addition to the crack opening, the distance to each neighboring crack was measured. These values were used as parameters in a plane-strain, finite-element model, using the appropriate elastic properties of the system, and assuming the three cracks penetrated to the interface between the topcoat and primer. The residual strain at room temperature was then deduced by calculating what strain would be required to match the finite-element results to the measured crack opening.

The opening of crack "2", shown in Fig. 6, was 98 nm. The finite-element calculations indicated that this opening for a crack, situated as it was between its two nearest neighbors, corresponded to a residual strain of 0.24%. The experiments and analyses were repeated for five different specimens loaded between 1.0% and 1.4%. There was no effect of applied strain on the calculated residual strain. This implies that the system was elastic, and that the crack opening was caused by residual strain, rather than plasticity. This residual strain was determined to be $0.22 \pm 0.02\%$ at room temperature.

For the tests conducted at elevated temperatures, the mismatch in thermal expansion between the substrate and the topcoat provides an additional component to the residual strain. The thermal-expansion coefficient of the polycarbonate substrate is 67.5×10^{-6} °C^{-1}, as given in the datasheet [26]. The thermal-expansion coefficient of the topcoat was determined using a Toho Technology FLX2320-S system to measure how the curvatures of 500 ± 25 μm thick, fused-quartz wafers coated with the topcoat varied with temperature, over the range 25 °C to 130 °C. The thickness of the topcoat in these experiments was 5.4 ± 0.1 μm. The thermal-expansion coefficient of fused quartz was assumed to be 5.5×10^{-7} °C^{-1}, resulting in a measured thermal-expansion coefficient for the topcoat of $32.1 \pm 1.1 \times 10^{-6}$ °C^{-1}. Neither the residual stresses nor the thermal expansion of the primer affect the mechanics of the problem, since the substrate was relatively thick, and the cracks terminated at the interface between the primer and topcoat.

3 Numerical Analysis

The experimental data for crack growth consisted of crack velocities measured as a function of effective strain and the distance between the two nearest neighbors. To convert these data to plots of crack velocity against energy-release rate required finite-element calculations for the energy-release rates at the tips of the growing cracks. These calculations were conducted using the measured distances to the nearest neighbors, the specific geometry and material properties of the system, and an assumption of linear elasticity.

A schematic illustration of the geometry assumed for this problem is shown in Fig. 7. There are three elastic layers: a topcoat of thickness h_t and plane-stress modulus E_t, a primer of thickness h_p and plane-stress modulus E_p, and a substrate of thickness h_s and plane-stress modulus E_s. A crack channels between two pre-existing flaws separated by a distance s, under an effective strain of ε_o, arising from both the residual tension and the applied strain. The propagating crack is located at a distance s_1 from its nearest neighbor. We made a further assumption that only the distances to the nearest neighbor on each side are important, and that the cracks are long enough to be propagating under steady-state conditions. Under these conditions, the energy-release rate can be calculated from a 2-D finite-element calculation, following the approach given in Refs. [2, 9]. The commercial finite-element program ABAQUS was used. Plane-strain elements were used, with a mesh-sensitivity analysis being performed to ensure that any numerical uncertainties were smaller than experimental uncertainties. The ratio of h_t/h_p was set to 4.37, and the ratio of h_t/h_s was set to 0.0020, to be consistent with the experimental geometry. The ratio of E_t/E_p was set to 0.66, and the ratio of E_t/E_s was set to 2.05. The Poisson's ratio for all three layers was set to a value of 0.37, which is the Poisson's ratio of the polycarbonate sheet given in [26].

The first step in determining the energy-release rate for channeling was to calculate the stress distribution through the thickness of the topcoat, at the location where the intermediate crack propagates (Fig. 8(a)). Examples of how this stress varies through the thickness of the topcoat are shown in Fig. 9 for different values of s_1/h_t, and for a fixed value of $s_1/s = 0.5$, corresponding to the mid-point between two pre-existing cracks. When the crack spacing is large enough, the stress distribution is approximately uniform. As s_1/h_t decreases, the stresses decrease, and become more non-uniform, even becoming negative on the surface in the extreme case of $s/h_t = 1$, owing to bending.

The second step in determining the energy-release rate for channeling was to compute the crack-opening displacement, $\delta_t(y)$, for a crack located at $x = s_1$ (Fig. 8(b)). The energy-release rate for channeling was then calculated from

$$\mathcal{G} = \frac{1}{2h_t} \int_0^{h_t} \sigma_t(y)\delta_t(y)dy \ . \tag{5}$$

This results in a non-dimensional expression for the energy-release rate of the form,

$$\frac{2\mathcal{G}}{\pi\varepsilon_o^2 \bar{E}_t h_t} = g\left(\tilde{\alpha}_t, \tilde{\beta}_t, \tilde{\alpha}_p, \tilde{\beta}_p, \frac{h_t}{h_p}, \frac{h_t}{h_s}, \frac{s}{h_t}, \frac{s_1}{s}, \right) \ . \tag{6}$$

where $\tilde{\alpha}_t$, $\tilde{\beta}_t$, $\tilde{\alpha}_p$, and $\tilde{\beta}_p$ are the two Dundurs' parameters for the topcoat and for the primer relative to the substrate, respectively.

Figure 10 illustrates how the energy-release rate varies with the crack spacing (s_1/s and s/h_t), for a set of material and geometrical properties corresponding to the current system of interest. These results were used to analyze the experiments. Every crack for which the velocity had been measured was identified by three parameters: the separation of its two nearest neighbors, s, the distance to its closest neighbor, s_1, and the effective strain, ε_o,

calculated from the measured applied strain and the estimated residual strain. From these three parameters, the energy-release rate was obtained from calculations similar to those presented in Fig. 10, and identified with the corresponding crack velocity. Details of these results are presented in the next section.

4 Results and discussion

The experimental observations and finite-element calculations described above were used to produce plots relating the crack velocity to the energy-release rate. The appropriate storage moduli for the coatings and the substrate (as given in Figs. 2 and 3) and the effects of thermal expansion (Section 2.4), at the temperature of each test, were included in the calculations. The results are summarized in Figs. 12 and 11. These figures show the effects of humidity (Fig. 11) and temperature (Fig. 12). The data were collected from 62 cracks on 14 samples at applied true strains ranging from $0.75\% \pm 0.03\%$ to $1.65\% \pm 0.05\%$. All the cracks had lengths that were more than 50 times greater than the topcoat thickness, so the assumptions of steady-state were met. As can be seen from Fig. 12, the threshold energy-release rate for channel cracking was 6.6 ± 0.8 J/m^2 at room temperature, with a lowest recorded velocity of 3.0 nm/s.

Figure 11 shows that the effects of humidity were negligible in this system over the range of the experiments studied. Figure 12 indicates that there was not a strong effect of temperature up to 65 ± 3 °C. However, the crack velocity appeared to be higher for the test at 89 ± 3 °C with the difference being more significant at higher energy-release rates. A slight decrease in the threshold energy-release rate was also observed at the highest temperature. The trends shown by these high-temperature data continued in few exploratory

and unreported experements conducted at 105 °C.

The nano-indentation DMA results of Fig. 2 indicate that the glass-transition temperature of the primer is about 90 °C. Therefore, at higher temperatures, it is possible that creep of the primer layer provides additional relaxation of the stresses when the topcoat cracks. This could increase the energy-release rate for channeling [11, 12] and, hence, increase the crack velocity for a given applied strain. In addition, Figure 13 shows that the cracks penetrated into the primer when tests were conducted at high temperatures. This is consistent with a drop in the modulus of the primer, and would also provide an additional contribution to the energy-release rate that was not included in the calculations used to generate the results of Fig. 12.

Although any effects of temperature are probably dominated by softening of the primer, which precludes being able to deduce a thermal activation energy for kinetic crack growth, it is of interest to see whether the form of Eqn. 4 is in general agreement with the experimental data. A curve fit of this equation to the data obtained at 25 $\pm$ 2 °C is provided in Fig. 14, with $A\exp(-Q/kT) = 0.22 \pm 0.08$ μm/s, and $B = 2.7 \pm 0.3 \times 10^{-21}$ m^2. It will be observed that this describes the data very well. If we further assume that the two in-plane, characteristic lengths for rupture are identical and equal to Δ, we get a value of $\Delta = 0.73 \pm 0.4$ Å for the topcoat, and a corresponding activation energy of $Q = 55 \pm 1$ kJ/mol (0.57 ± 0.01 eV / bond). While the characteristic length, in particular, seems to be a bit low, these values are certainly within a reasonable range of the values one might expect for rupture of a polymeric film.

To investigate whether there is any fatigue crack growth in this system, the average crack velocity was measured for three cracks, each being tested at three different fatigue

frequencies (1, 2 and 5 Hz) at 24 ± 1 ^{o}C. The average velocities at each frequency were then compared to the velocities that would be predicted by integrating Eqn. 4 (with the experimentally measured values) over each cycle. The results are provided in Table 1, from which it will be seen that there was no obvious effect of frequency on crack velocity at room temperature. Plastic ratcheting in a primer layer or substrate [27, 28] has been invoked to explain effects of fatigue in brittle coatings [29, 30, 31]. However, it appears that the primer is sufficiently brittle in this system, at room temperature, to avoid fatigue effects. We did not explore the possibility of fatigue at higher temperatures, where the primer may be above its glass-transition temperature.

5 Conclusions

In this paper we have demonstrated a technique to analyze the velocity of channeling cracks in coatings and thin films, as a function of energy-release rate. This technique relies on a recognition of how the energy-release rate of a channeling crack is very sensitive to the depth to which it penetrates, its interactions with neighboring cracks, and the geometry and material properties of the system. The approach requires verification of the crack depth to determine through how many layers the crack penetrates. This can be done by focused ion-beam milling followed by electron microscopy. The energy-release rate has to be calculated for individual cracks, using finite-element calculations and the measured distances from their nearest neighbors. The levels of residual strain in the cracked layer also need to be determined. This can be done by measuring the crack-opening displacements of cracks at known distances from their neighbors, and comparing them to numerical calculations.

These techniques have been used to explore the time-dependent crack propagation in a

polymeric nano-composite system used as a hard coating on polycarbonates for automotive glazing applications. It was demonstrated that the particular system exhibited neither fatigue-crack growth, nor stress-corrosion cracking. Furthermore, the form of the velocity / energy-release rate curve was not consistent with models of visco-elastic crack growth. However, the behavior did fit a thermally-activated fracture process, with a very low threshold toughness of about 7 J/m^2, with an estimated activation energy of about 0.6 eV/bond.

Acknowledgements

FM and MDT gratefully acknowledge support for this project from Ford Motor Company and Momentive Performance Materials.

References

[1] M. E. Nichols and C. A. Peters. The effect of weathering on the fracture energy of hardcoats over polycarbonate. *Polymer Degradation and Stability*, 75(3):439–446, 2002.

[2] J. L. Beuth Jr. Cracking of thin bonded films in residual tension. *International Journal of Solids and Structures*, 29(13):1657–1675, 1992.

[3] J. J. Vlassak. Channel cracking in thin films on substrates of finite thickness. *International Journal of Fracture*, 119(4):299–323, 2003.

[4] J. Dundurs. Edge-bonded dissimilar orthogonal elastic wedges. *Journal of Applied Mechanics*, 36:650–652, 1969.

[5] M. D. Thouless. Crack spacing in brittle films on elastic substrates. *Journal of the American Ceramic Society*, 73(7):2144–2146, 1990.

[6] M. D. Thouless, E. Olsson and A. Gupta. Cracking of brittle films on an elastic substrate. *Acta Metallurgica et Materialia*, 40(6):1287–1292, 1992.

[7] J. W. Hutchinson and Z. Suo. Mixed mode cracking in layered materials. *Advances in Applied Mechanics*, 29(63):191, 1992.

[8] V. B. Shenoy, A. F. Schwartzman and L. B. Freund. Crack patterns in brittle thin films. *International Journal of Fracture*, 103(1):1–17, 2000.

[9] M. D. Thouless, Z. Li, N. J. Douville and S. Takayama. Periodic cracking of films supported on compliant substrates. *Journal of the Mechanics and Physics of Solids*, 59(9):1927–1937, 2011.

[10] S. Takayama J. Huang, B. C. Kim and M. D. Thouless. The control of crack arrays in thin films. *Journal of Materials Science*, 49(1):255–268, 2014.

[11] R. Huang, J. H. Prévost and Z. Suo. Loss of constraint on fracture in thin film structures due to creep. *Acta Materialia*, 50(16):4137–4148, 2002.

[12] J. Liang, R. Huang, J. H. Prévost and Z. Suo. Thin film cracking modulated by underlayer creep. *Experimental Mechanics*, 43(3):269–279, 2003.

[13] A. S. Wineman and K. R. Rajagopal. *Mechanical Response of Polymers: An Introduction*. Cambridge University Press, Cambridge, UK, 2000.

[14] H. Wang, W. Lu, J. R. Barber and M. D. Thouless. The roles of cohesive strength and toughness for crack growth in visco-elastic and creeping materials,. *Engineering Fracture Mechanics*, 160:226–237, 2016.

[15] S. M. Wiederhorn. Influence of water vapor on crack propagation in soda-lime glass. *Journal of the American Ceramic Society*, 50(8):407–414, 1967.

[16] T. Y. Tsui, A. J. McKerrow and J. J. Vlassak. Constraint effects on thin film channel cracking behavior. *Journal of Materials Research*, 20(9):2266–2273, 2005.

[17] K. Kim, H. Luo, A. K. Singh, T. Zhu, S. Graham, and O. N. Pierron. Environmentally assisted cracking in silicon nitride barrier films on poly(ethylene terephthalate) substrates. *Applied Materials and Interfaces*, 8:27169–27178, 2016.

[18] K. Kim, S. Graham, and O. N. Pierron. Note: A single specimen channel crack growth technique applied to brittle thin films on polymer substrates. *Review of Scientific Instruments*, 88:036102, 2017.

[19] M. W. Lane, J. M. Snodgrass and R. H. Dauskardt. Environmental effects on interfacial adhesion. *Microelectronics Reliability*, 41(9):1615–1624, 2001.

[20] J. J. Vlassak, Y. Lin and T. Y. Tsui. Fracture of organosilicate glass thin films: Environmental effects. *Materials Science and Engineering: A*, 391(1):159–174, 2005.

[21] E. P. Guyer and R. H. Dauskardt. Fracture of nanoporous thin-film glasses. *Nature Materials*, 3(1):53–57, 2004.

[22] R. F. Cook and E. G. Liniger. Kinetics of indentation cracking in glass. *Journal of the American Ceramic Society*, 76(5):1096–1105, 1993.

[23] B. R. Lawn. *Fracture of Brittle Solids*. Cambridge University Press, Cambridge, UK, 1993.

[24] S. M. Wiederhorn, H. Johnson, A. M. Diness and A. H. Heuer. Fracture of glass in vacuum. *Journal of the American Ceramic Society*, 57(8):336–341, 1974.

[25] B. R. Lawn. An atomistic model of kinetic crack growth in brittle solids. *Journal of Materials Science*, 10(3):469–480, 1975.

[26] Lexan^{TM} 9034 product data sheet, 2012.

[27] M. Huang, Z. Suo and Q. Ma. Plastic ratcheting induced cracks in thin film structures. *Journal of the Mechanics and Physics of Solids*, 50(5):1079–1098, 2002.

[28] Z. Suo, J. J. Vlassak and S. Wagner. Micromechanics of macroelectronics. *China Particuology*, 3(6):321–328, 2005.

[29] D. R. Cairns and G. P. Crawford. Electromechanical properties of transparent conducting substrates for flexible electronic displays. *Proceedings of the IEEE*, 93(8):1451–1458, 2005.

[30] M. R. Begley and A. G. Evans. Progressive cracking of a multilayer system upon thermal cycling. *Journal of Applied Mechanics*, 68(4):513–520, 2000.

[31] M. Huang, Z. Suo, Q. Ma and H. Fujimoto. Thin film cracking and ratcheting caused by temperature cycling. *Journal of Materials Research*, 15(6):1239–1242, 2000.

Table 1: Comparisons between measured crack velocities under cyclic loading and the velocities predicted by integration of Eqn. 4 over a cycle. The observations and predictions are essentially identical. Furthermore, there was no significant effect of loading frequency on crack velocity. These results indicate that fatigue was not a significant factor for room-temperature crack propagation in this system.

Crack 1

Frequency (Hz)	Measured crack velocity (μm/s)	Predicted average crack velocity in each cycle (μm/s)
1	0.12 ± 0.02	0.14 ± 0.05
2	0.11 ± 0.05	0.14 ± 0.05
5	0.09 ± 0.03	0.13 ± 0.04

Crack 2

Frequency (Hz)	Measured crack velocity (μm/s)	Predicted average crack velocity in each cycle (μm/s)
1	0.15 ± 0.05	0.16 ± 0.06
2	0.13 ± 0.04	0.16 ± 0.06
5	0.10 ± 0.03	0.14 ± 0.05

Crack 3

Frequency (Hz)	Measured crack velocity (μm/s)	Predicted average crack velocity in each cycle (μm/s)
1	0.19 ± 0.03	0.18 ± 0.07
2	0.16 ± 0.03	0.18 ± 0.07
5	0.14 ± 0.02	0.16 ± 0.06

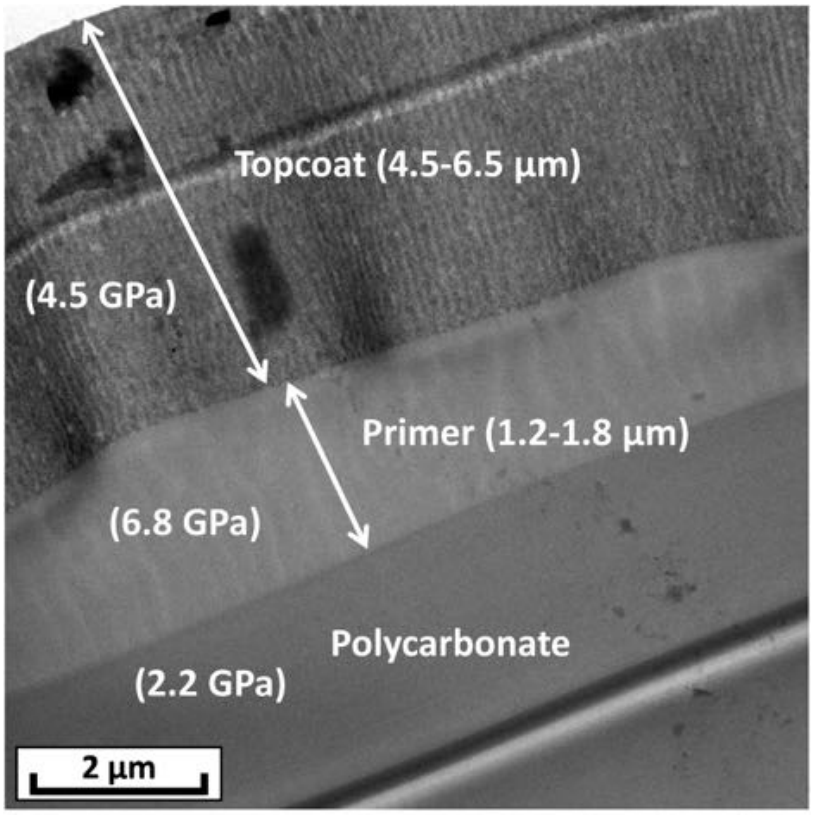

Figure 1: The system studied in this paper consists of a clear polycarbonate substrate, a polyacrylate-type primer, and a silicone topcoat containing colloidal silica.

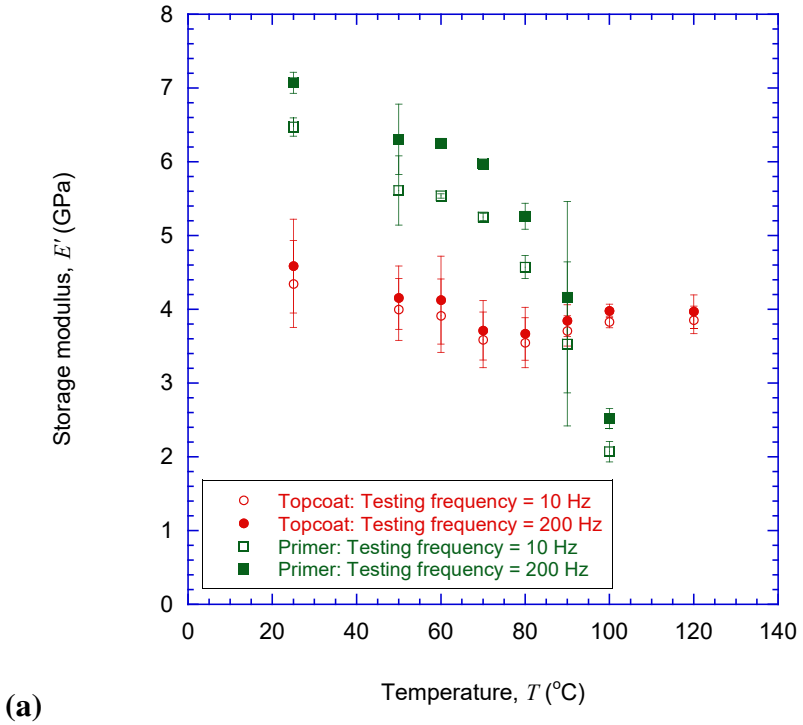

(a)

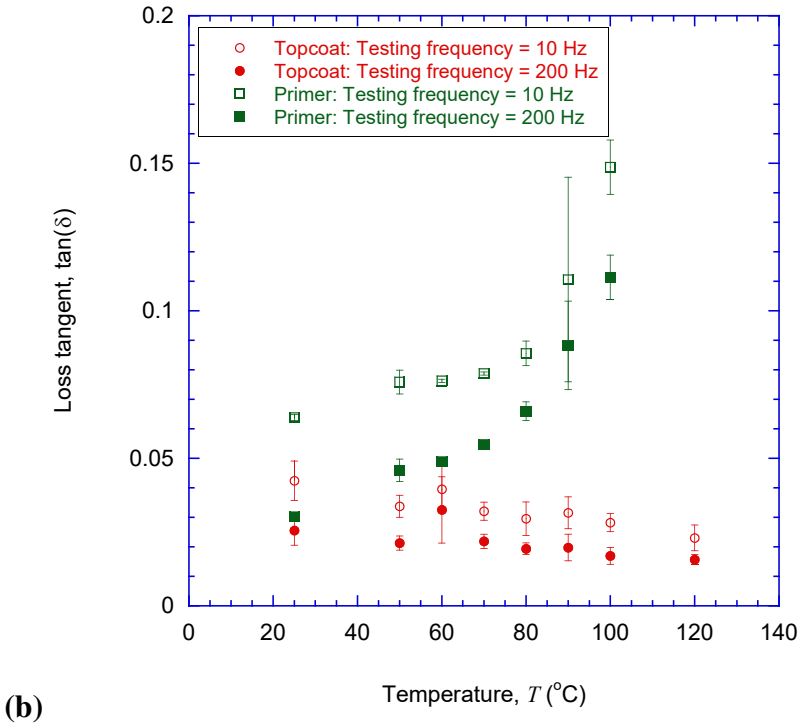

(b)

Figure 2: Dynamic indentation temperature sweeps for the topcoat and primer: **(a)** storage modulus, and **(b)** loss tangent. The glass-transition temperature of the primer is about 90 °C, in this frequency range. The glass-transition temperature for the topcoat appears to be at least higher than 130 °C.

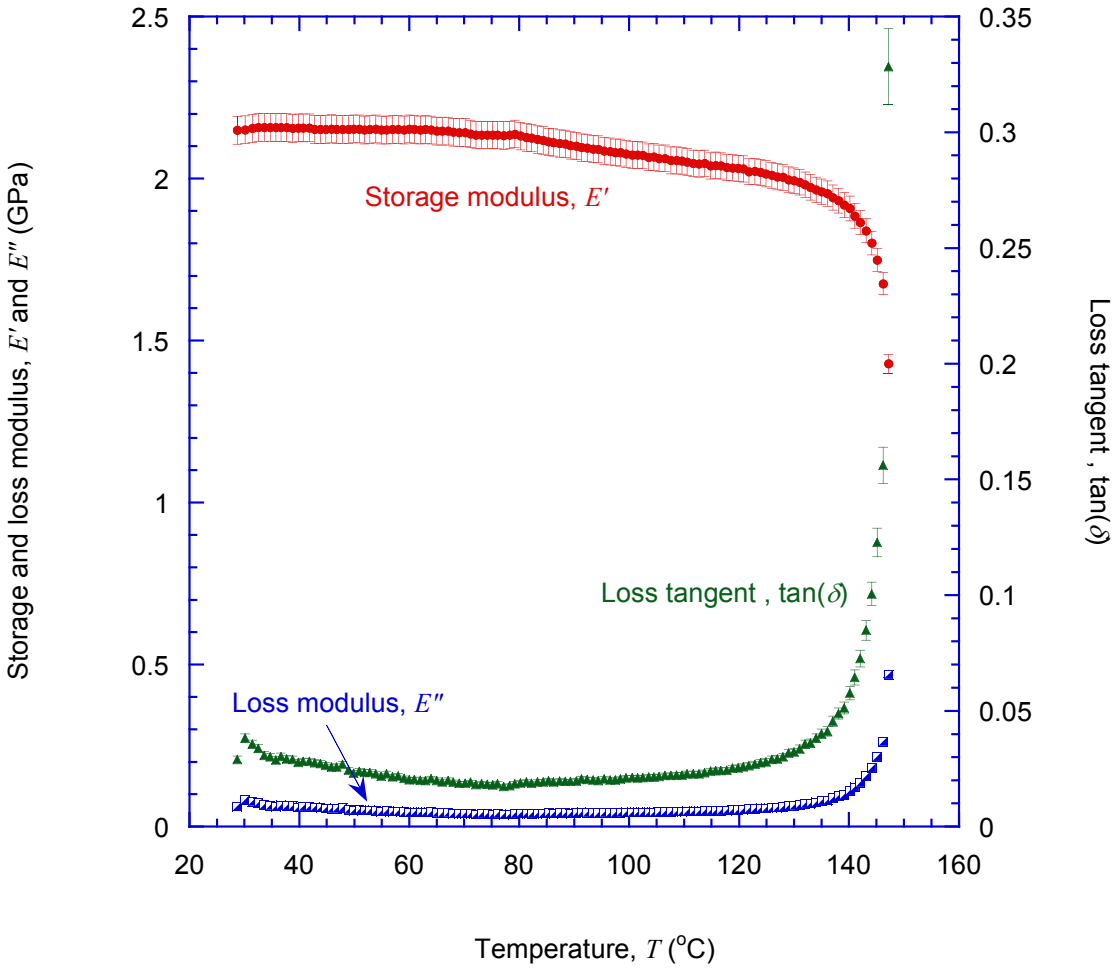

Figure 3: Typical temperature sweep at a frequency of 1 Hz for the polycarbonate substrate. The storage modulus, loss modulus and loss tangent exhibited a limited temperature dependence below 135 ^{o}C. Above this temperature, there was a dramatic decrease in the storage modulus, and a corresponding increase in the loss modulus and loss tangent.

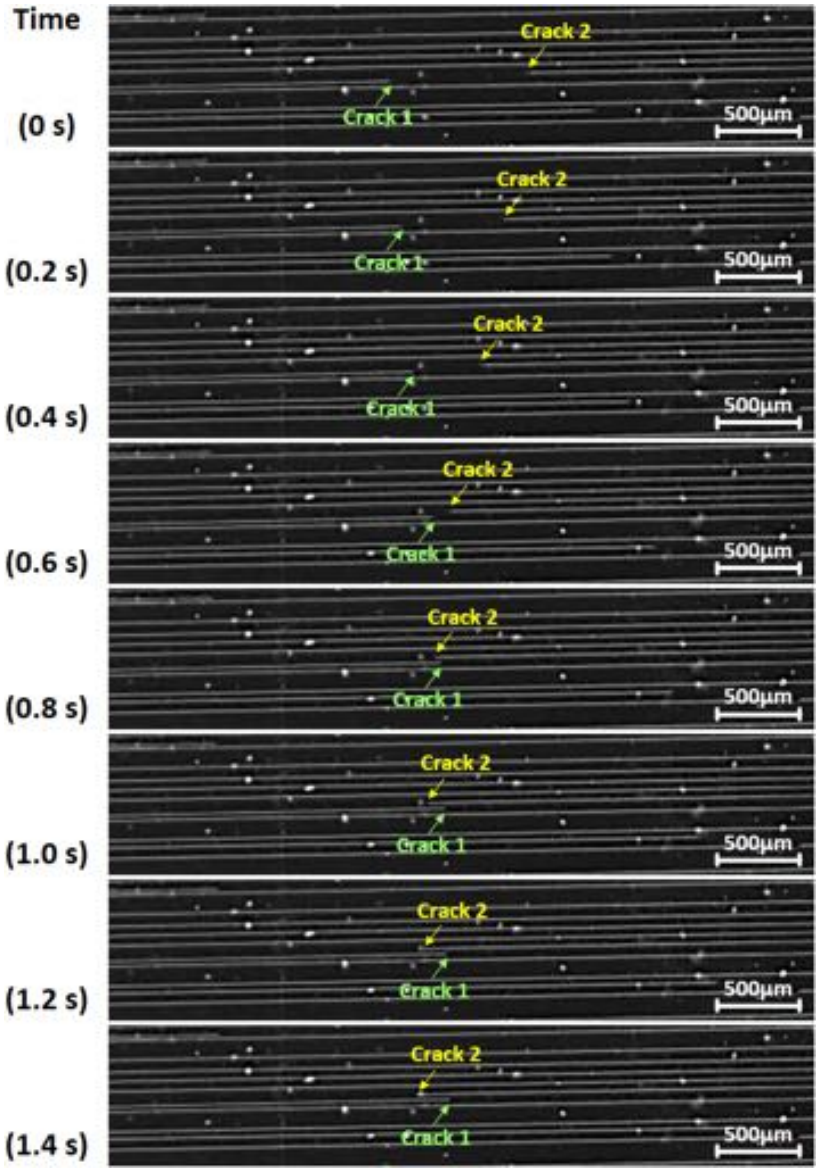

Figure 4: A sequence of images at 0.2 s intervals for two cracks (with tips labeled "1" and "2") propagating between two existing cracks. The energy-release rate depends on the distance of a propagating crack from its two nearest neighbors. For a given level of effective strain, the energy-release rate (and crack velocity) is higher when the spacing is larger. It can be seen that the two cracks slowed down after they passed each other, because their own interaction formed new nearest neighbors for each of them. This figure was taken at an applied strain of 1.58%.

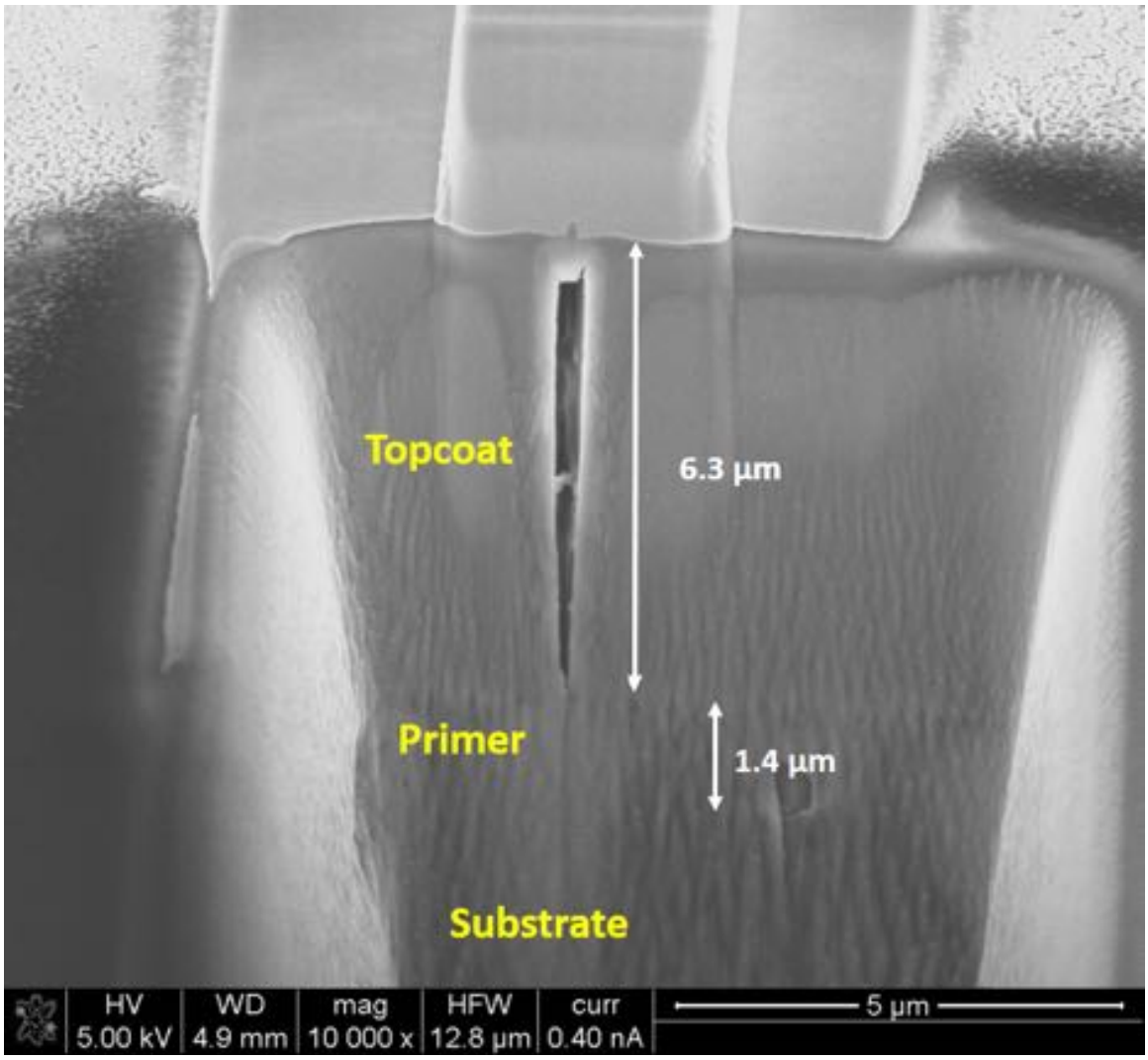

Figure 5: A scanning-electron micrograph of a channeling crack formed at room temperature, taken in cross-section from a sample with a 6.3 μm topcoat and a 1.4 μm primer in thickness. This image shows that the channeling cracks terminated at the interface between the topcoat and primer.

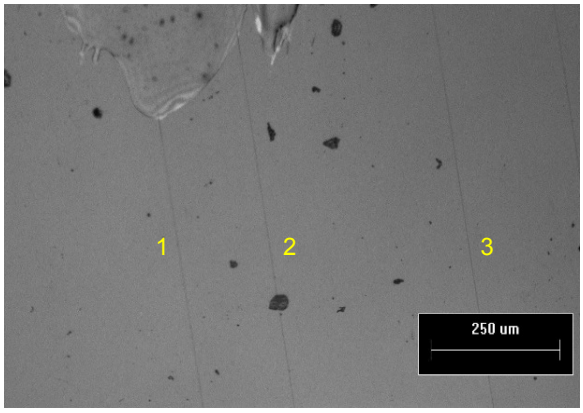

(a)

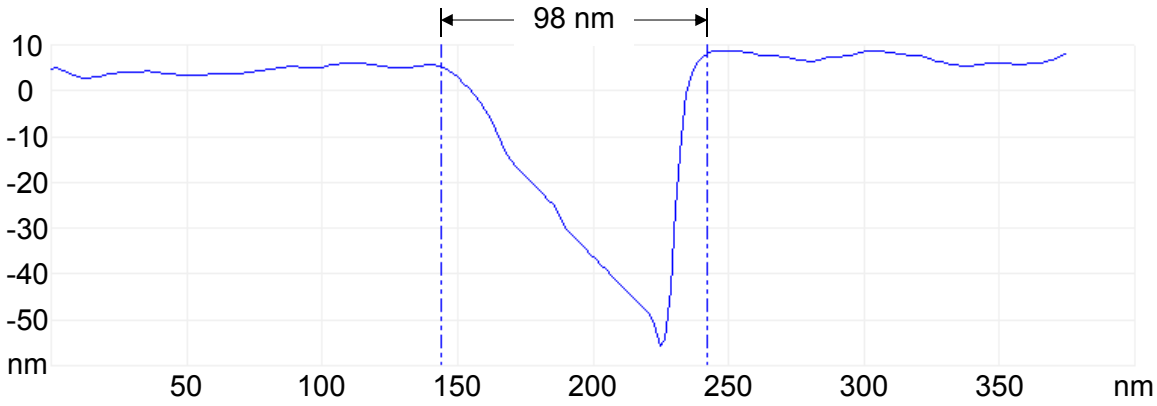

(b)

Figure 6: **(a)** Three cracks were selected for analysis from a sample that had been strained to 1.03 %. The distances from the central crack to its nearest neighbors were measured, and used as parameters for the numerical model shown in Fig. 8. **(b)** The opening at the surface of the topcoat of the center crack labelled as "2" was measured by AFM to be 98 nm. The numerical analysis then indicated that the residual strain that would result in such an opening is $0.24 \pm 0.02\%$.

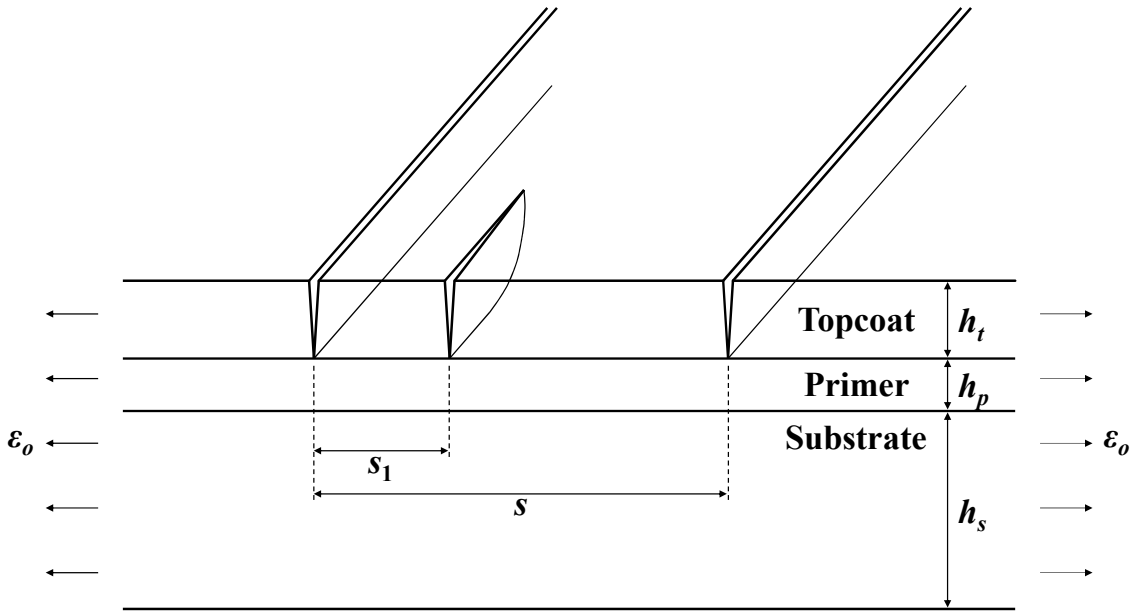

Figure 7: A schematic of the problem discussed in this paper. The system has three layers with two thin films (called topcoat and primer in this paper) on top of a substrate. A crack propagates in the topcoat between two pre-existing cracks, under an effective tensile strain of ε_o, which consists of strain applied to the substrate plus an additional residual strain within the topcoat. The two pre-existing cracks are at a distance of s apart, and the distance between the channeling crack and its closest neighbor is s_1.

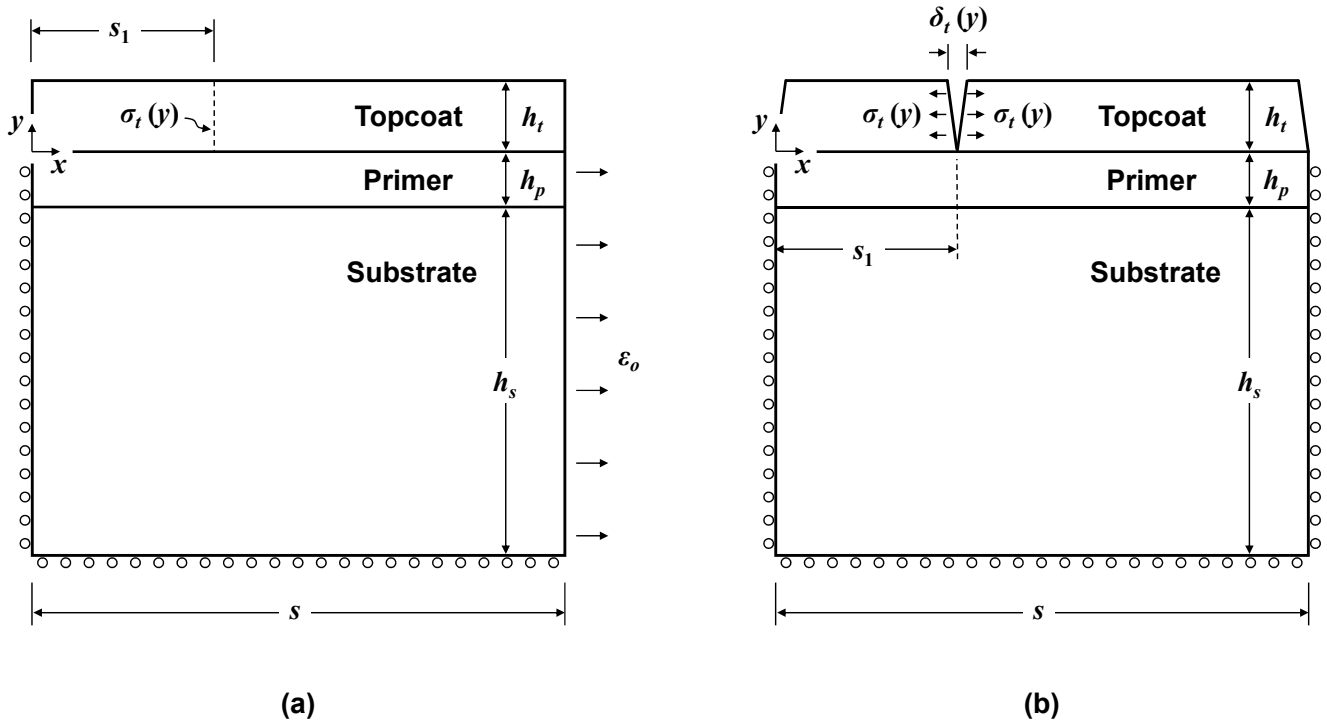

Figure 8: Energy-release rate of crack between two neighbors can be calculated by comparing the change in strain energy of a segment of the system as a crack passes through it. Specifically, the calculation was done by **(a)**calculating the stress $\sigma_t(y)$ in the un-cracked topcoat system at the location where the crack propagates and **(b)** computing the crack-opening, $\delta_t(y)$, after the crack has passed through this plane, by applying the stress distribution obtained in (a) but in opposite direction on the crack surface.

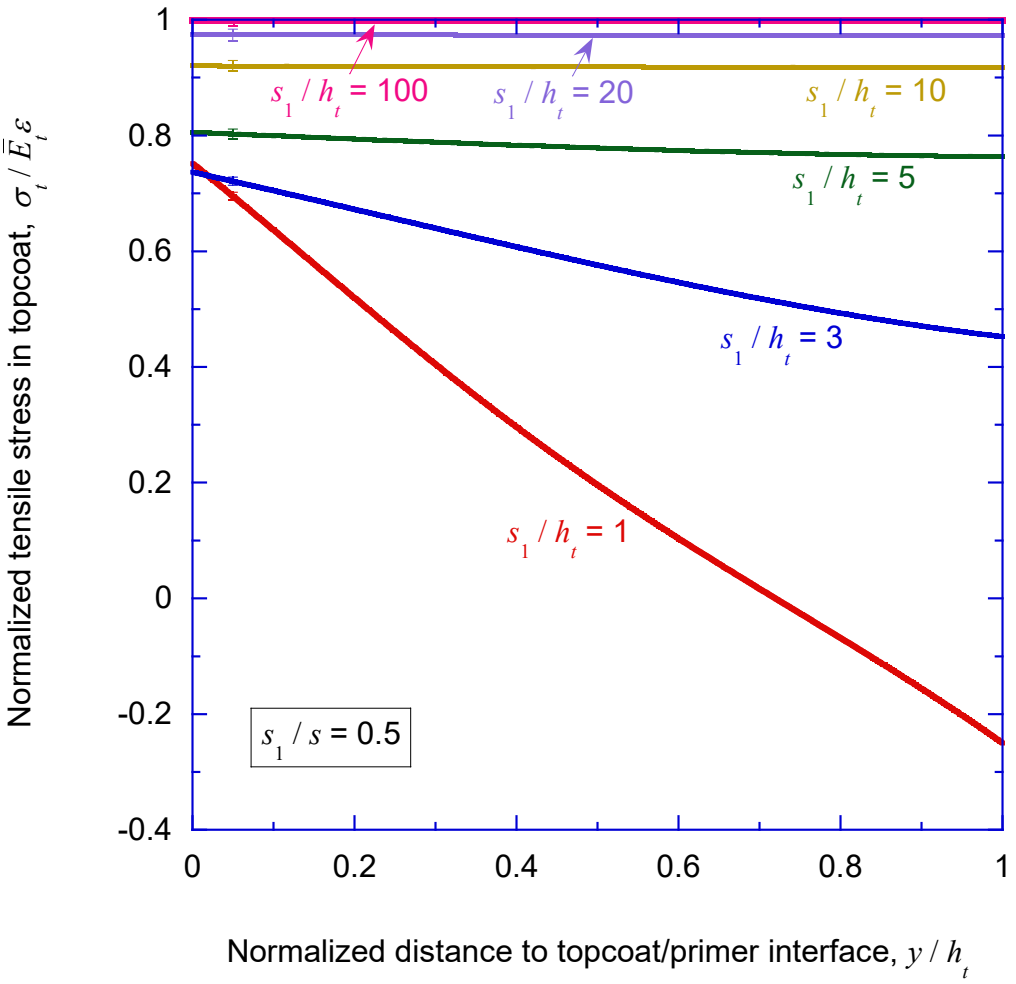

Figure 9: The stress in the film as a function of distance from the interface between the topcoat and primer interface to the free surface. The stresses have been plotted for a fixed value of the ratio $s_1/s = 0.5$, but for different values of s_1/h_t. The stresses have been normalized by the product of the plane-strain modulus of the topcoat ($\bar{E}_t$) and the effective strain in the topcoat of ϵ_o. The other non-dimensional geometrical and material parameters in these calculations were set to $E_t/E_p = 0.66$, $E_t/E_s = 2.05$, $h_t/h_p = 4.37$, $h_t/h_s = 0.0020$, and $\nu = 0.37$ for all three layers.

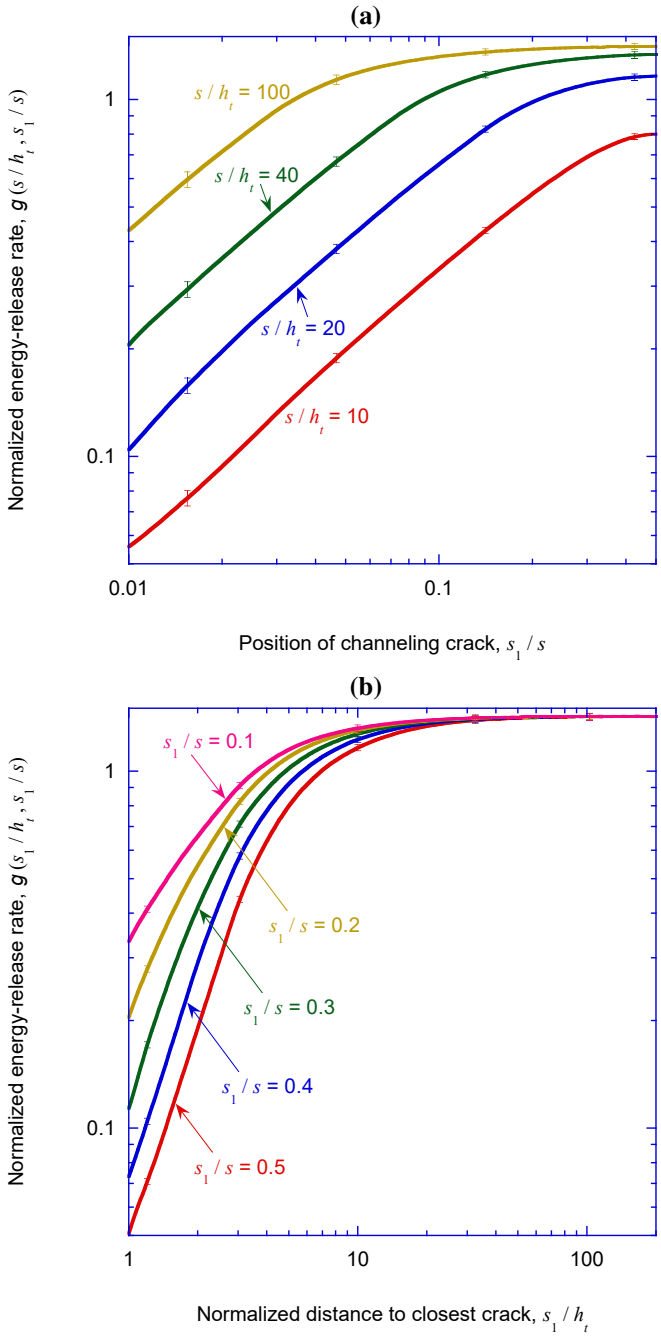

Figure 10: Plots showing how the normalized energy-release rate, $g = \mathcal{G}/(\epsilon_o^2 \bar{E}_t h_t)$ depends on the distance to the neighbors. The geometrical and material non-dimensional groups are the same as in Fig. 9. **(a)** As expected, the energy-release rate is highest when the crack propagates at the mid-point between its two neighbors ($s_1/s = 0.5$). **(b)** If s_1/h_t is greater than about 20, the energy-release rate is equal to that of an isolated crack channeling across the film, and independent of the crack spacing s_1/s. However, for values of s_1/h_t less than about 10, the energy-release rate is very sensitive to the spacing, and accurate interpretation of the experimental data requires the spacing to be known reasonably accurately.

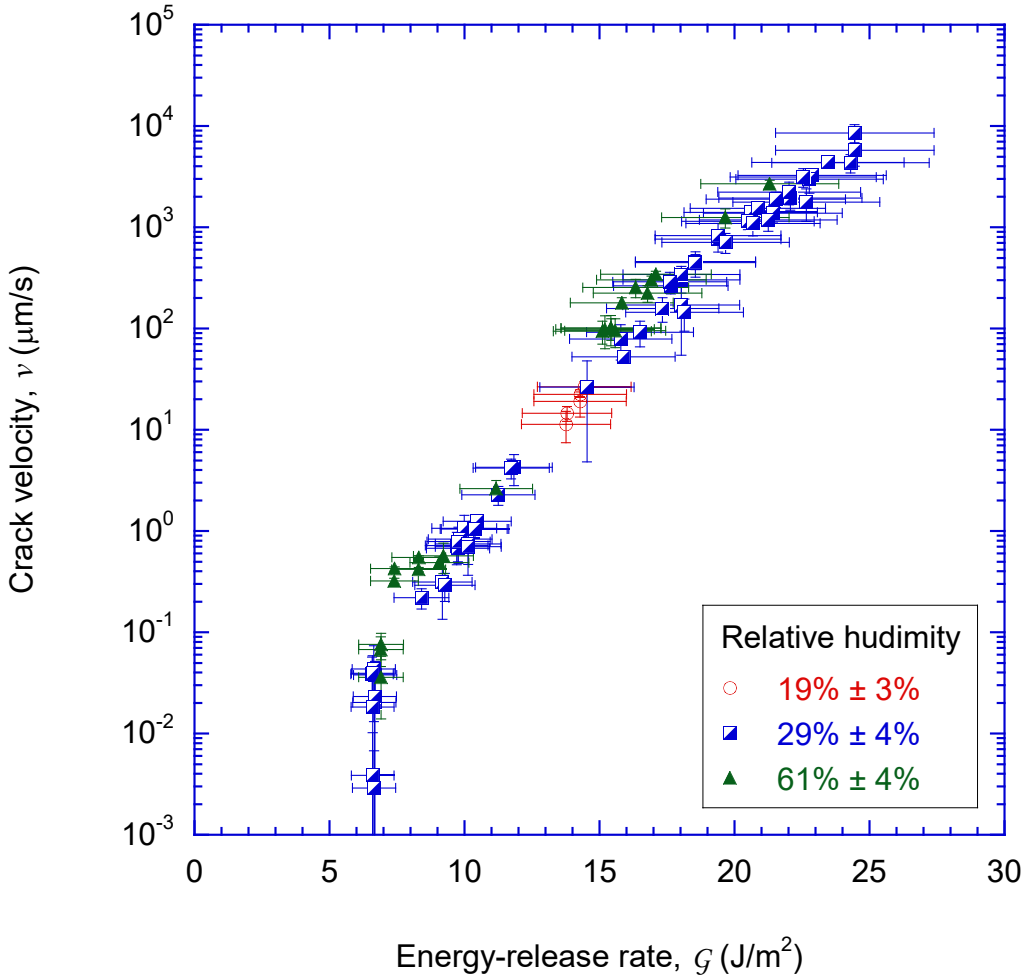

Figure 11: The crack velocity - energy-release rate curves at room temperature of 25 ± 2 °C, and relative humidities of $19 \pm 3\%$, $29 \pm 4\%$ and $61 \pm 4\%$. Within the uncertainties of the experiment, there were no obvious discrepancies between these curves, showing that in this range, the relative humidity did not have a significant effect on the crack velocity.

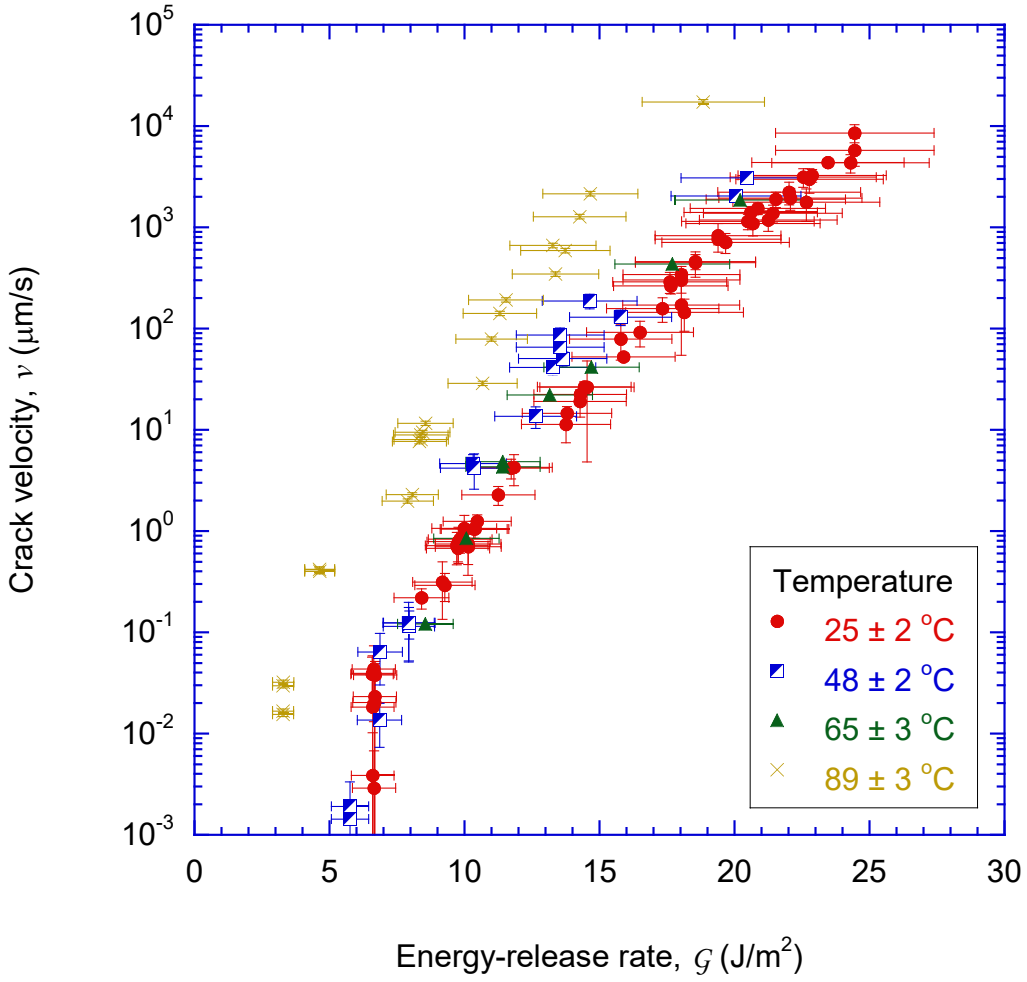

Figure 12: The results of the finite-element calculations (Section 3) were used with the experimental observations of crack spacing and velocity described in Section 2.2 to construct a graph of how the crack velocity depends on energy-release rate at temperatures of 25 ± 2 °C, 48 ± 2 °C, 65 ± 3 °C and 89 ± 3 °C. The relative humidity varied between 16% and 33%.

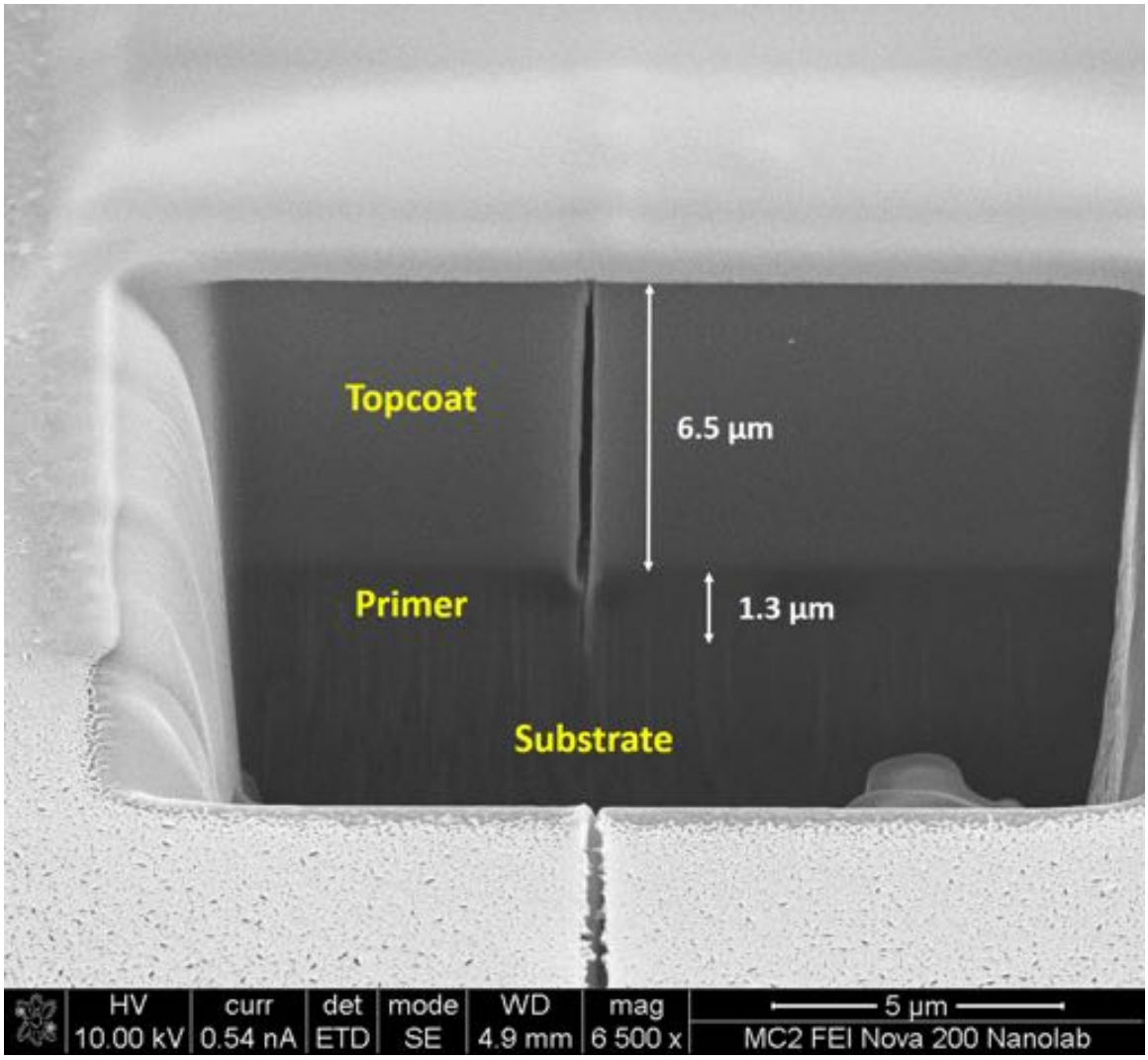

Figure 13: A scanning-electron micrograph of a cross-section through the topcoat and primer where a crack had channeled across the sample at a temperature 89 ± 3 °C. It will be noted that there is evidence of flow in the primer, and the crack tip has penetrated into the primer. This figure should be contrasted with Fig. 5, corresponding to cracking at room temperature.

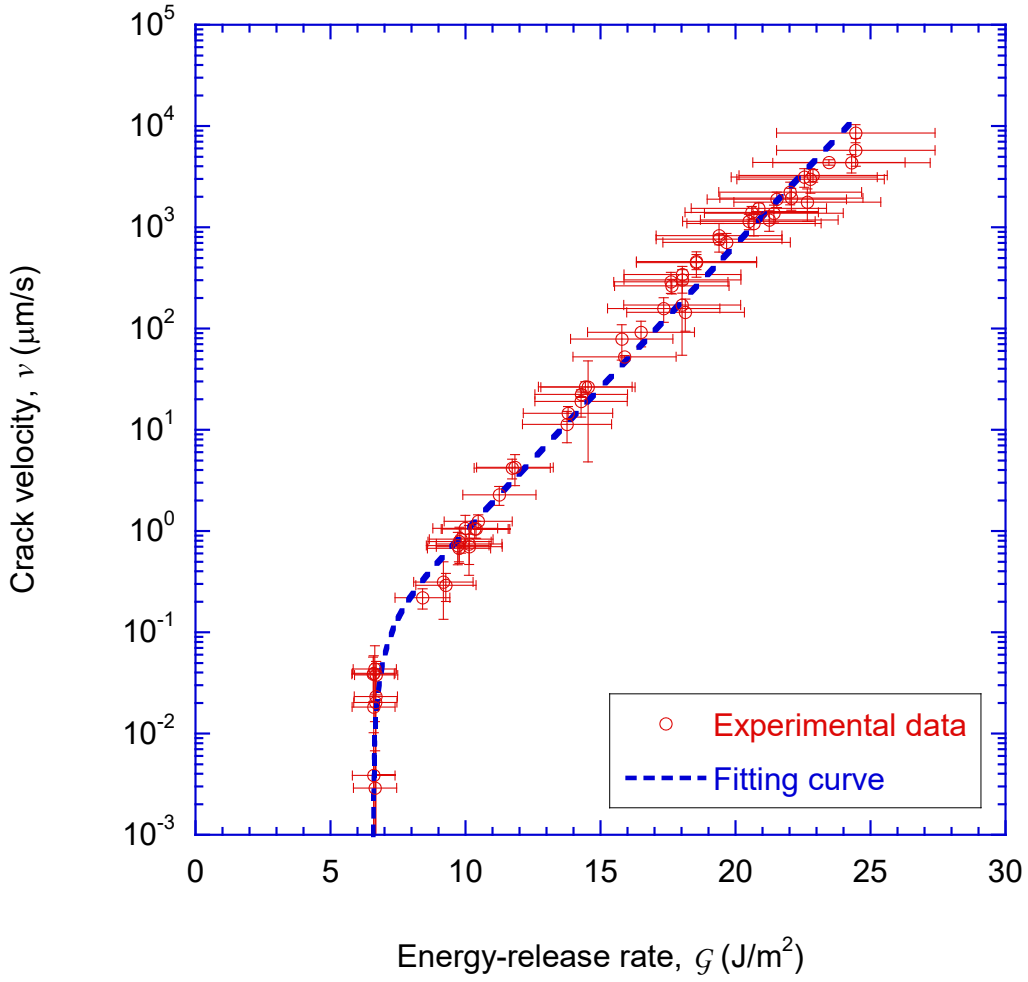

Figure 14: The data of Fig. 11 fitted to kinetic-rupture model of Eqn. 4, with $A\exp(-Q/kT)$ and B/kT having the values of 0.22 ± 0.08 μm/s and 0.65 ± 0.07 m^2/J respectively.